ARMY RESEARCH LABORATORY

XCT Study of Cone Crack Damage in Multilayered Transparent Panel Structures and Comparison to Modeling

by William H. Green, Raymond E. Brennan, and Costas F. Fountzoulas

ARL-TR-6082 **August 2012**

NOTICES

Disclaimers

The findings in this report are not to be construed as an official Department of the Army position unless so designated by other authorized documents.

Citation of manufacturer's or trade names does not constitute an official endorsement or approval of the use thereof.

Destroy this report when it is no longer needed. Do not return it to the originator.

Army Research Laboratory
Aberdeen Proving Ground, MD 21005-5069

ARL-TR-6082 **August 2012**

XCT Study of Cone Crack Damage in Multilayered Transparent Panel Structures and Comparison to Modeling

William H. Green, Raymond E. Brennan, and Costas F. Fountzoulas
Weapons and Materials Research Directorate, ARL

REPORT DOCUMENTATION PAGE	*Form Approved OMB No. 0704-0188*

1. REPORT DATE *(DD-MM-YYYY)*	2. REPORT TYPE	3. DATES COVERED (From - To)
August 2012	Final	January 2011–January 2012

4. TITLE AND SUBTITLE
XCT Study of Cone Crack Damage in Multilayered Transparent Panel Structures and Comparison to Modeling

5a. CONTRACT NUMBER

5b. GRANT NUMBER

5c. PROGRAM ELEMENT NUMBER

6. AUTHOR(S)
William H. Green, Raymond E. Brennan, and Costas F. Fountzoulas

5d. PROJECT NUMBER
622105H84RK02

5e. TASK NUMBER

5f. WORK UNIT NUMBER

7. PERFORMING ORGANIZATION NAME(S) AND ADDRESS(ES)
U.S. Army Research Laboratory
ATTN: RDRL-WMM-D
Aberdeen Proving Ground, MD 21005-5069

8. PERFORMING ORGANIZATION REPORT NUMBER
ARL-TR-6082

9. SPONSORING/MONITORING AGENCY NAME(S) AND ADDRESS(ES)

10. SPONSOR/MONITOR'S ACRONYM(S)

11. SPONSOR/MONITOR'S REPORT NUMBER(S)

12. DISTRIBUTION/AVAILABILITY STATEMENT
Approved for public release; distribution is unlimited.

13. SUPPLEMENTARY NOTES

14. ABSTRACT
Transparent and opaque materials are used by the U.S. Army in protective systems for enhancing survivability of ground vehicles, air vehicles, and personnel. Transparent materials are utilized for face shields, riot gear, and vehicle windows, in addition to other applications for sensor protection, including radomes and electromagnetic windows. Fracture from low-velocity impacts limits visibility and impairs continued vehicle operations. Transparent protective systems typically consist of glass, polymeric, and ceramic materials. Impact damage in different multilayered transparent panel structure types was investigated using a number of nondestructive evaluation methods, including phased array ultrasonic testing and x-ray computed tomography (XCT). Some of the damaged specimens exhibited multiple cone cracks in the second glass layer in front of the backing plate. The spatial characteristics of cone cracks were analyzed using geometric data from the XCT scans (images). Quantitative calculations on the extent of the cone spans were performed. Physical cone attributes (e.g., cone angle) were compared to crack damage geometries generated by theoretical simulations of impact damage.

15. SUBJECT TERMS
transparent, multilayered, cone cracks, NDE, x-ray computed tomography, XCT, modeling

16. SECURITY CLASSIFICATION OF:			17. LIMITATION OF ABSTRACT	18. NUMBER OF PAGES	19a. NAME OF RESPONSIBLE PERSON
a. REPORT	b. ABSTRACT	c. THIS PAGE			William H. Green
Unclassified	Unclassified	Unclassified	UU	26	19b. TELEPHONE NUMBER (*Include area code*) 410-306-0817

Contents

List of Figures iv

List of Tables v

1. Introduction 1

2. Description of Specimens and Digital Radiography Scans 1

3. XCT Scanning Procedures 2

4. XCT Evaluation of Specimens 3

5. Description of Damage Modeling 10

6. Comparison of Modeling to XCT Scans 11

7. Conclusions 14

8. References 15

Distribution List 17

List of Figures

Figure 1. Through-thickness DRs: (a) specimen 740-1 and (b) specimen 741-2. 2

Figure 2. Impact cavity centerline XCT scans (images): (a) specimen 740-1, (b) specimen 740-2, (c) specimen 741-1, and (d) specimen 741-2. 3

Figure 3. Enlarged XCT scans of specimen 740-1: (a) centerline, (b) 7.7 mm above centerline, and (c) 19.2 mm below centerline. 4

Figure 4. Enlarged XCT scans of specimen 741-2: (a) centerline and (b–i) 3.6 mm above centerline, 7.2 mm above, 15.0 mm above, 25.6 mm above, 3.6 mm below, 7.2 mm below, 15.0 mm below, and 25.4 mm below. 4

Figure 5. Centerline XCT scan of specimen 740-1, with defining locations of internal crater and cracks marked (arrows). 5

Figure 6. Centerline XCT scan of specimen 741-2, with defining locations of internal crater and cracks marked (arrows). 6

Figure 7. Three-dimensional isometric views of in-plane curvilinear sections of the main cone crack in specimen 740-1: (a) faces of plates displayed as transparent and (b) front surface of middle plate displayed as opaque. 7

Figure 8. Three-dimensional isometric views of fitted surfaces through the main cone crack in specimen 740-1: (a) meshed surface and (b) solid surface. 7

Figure 9. Three-dimensional isometric views of in-plane curvilinear sections of cone cracks in specimen 741-2: (a) all mapped curvilinear sections, (b) only sections of frontal cone crack, (c) only sections of second cone crack, and (d) specific faces of plates are displayed as opaque. 9

Figure 10. Three-dimensional isometric views of fitted surfaces through cone cracks in specimen 741-2: (a) meshed surface through frontal cone crack, (b) solid surface through frontal cone crack, (c) solid surface through second cone crack, (d) frontal and second cone crack, and (e) rear view of frontal and second crack. 10

Figure 11. Side-by-side comparison of modeled damage “slices” and XCT scans of specimen 740-1: (a–f) modeled damage and (g–i) XCT scans. 12

Figure 12. Side-by-side comparison of modeled damage slices and XCT scans of specimen 741-2: (a–g) modeled damage and (h–n) are XCT scans. 13

List of Tables

Table 1. Specific crack and crater locations in specimen 740-1. 5
Table 2. Specific crack and crater locations in specimen 741-2. 6

INTENTIONALLY LEFT BLANK.

1. Introduction

Nondestructive evaluation (NDE) or nondestructive testing is a discipline of materials science that encompasses a wide variety of inspection modalities. NDE is applicable to an extremely wide variety of materials, components, and systems and is utilized to inspect objects at the surface, subsurface, and in the interior. X-ray computed tomography (XCT) scanning is a through-penetration method used for the evaluation and analysis of internal geometrical and physical characteristics of materials. XCT scanning has been used to characterize armor ceramics, including ballistically damaged ceramics (*1–6*), and to characterize and evaluate ballistically damaged encapsulated ceramic panels (*7, 8*). XCT scanning, as well as other NDE methods, has been used to characterize low-velocity projectile damage in transparent ceramic panel structures (*9–11*). In the first part of this work, two different types of multilayered panel structures were studied. The study was performed to compare the relative performance of different transparent materials used for the strike face of the structures against low-velocity impact damage. The first type of panel structure used a thicker, relatively typical transparent material for the strike face panel. The second type of panel structure used a thinner, novel transparent material for the strike face panel. This report will show and discuss the characterization of the cone cracks in two specimens from the study. Comparisons of XCT scans to three-dimensional (3-D) theoretical simulations of material damage will be made.

2. Description of Specimens and Digital Radiography Scans

Each of the two specimens consists of three 14- × 14-in transparent ceramic plates with adhesive between them to bond them together. The specimens were identified as 740-1 and 741-2. The middle and last layer (backing plate) of each specimen was the same, with the first layer (strike face) being different. The strike face plates of 740-1 and 741-2 were a conventional transparent material and a thinner new transparent material, respectively. Specimens 740-1 and 741-2 were struck by a 19.05-mm diameter steel sphere, with an impact velocity of 32.4 m/s, and a 5.56-mm diameter steel sphere, with an impact velocity of 405 m/s, respectively. Two-dimensional projection digital radiographs (DRs) are commonly taken before XCT scans to find overall differences in a specimen and aid in determining specific XCT scan locations. Digital radiographs of each specimen were taken through their thickness using the 420-keV x-ray tube and linear detector array (LDA) setup in translate-rotate (TR) mode. The x-ray technique parameters of the DRs were 400 keV and 2.0 mA. Geometries of source-to-object distance (SOD) = 649.74 mm and source-to-image-distance (SID) = 948.83 mm. Figure 1 shows digital radiographs of each specimen, where the partial penetration or impact cavity in each image is evident. Some of the cracks with large enough widths around the impact cavities are visible in

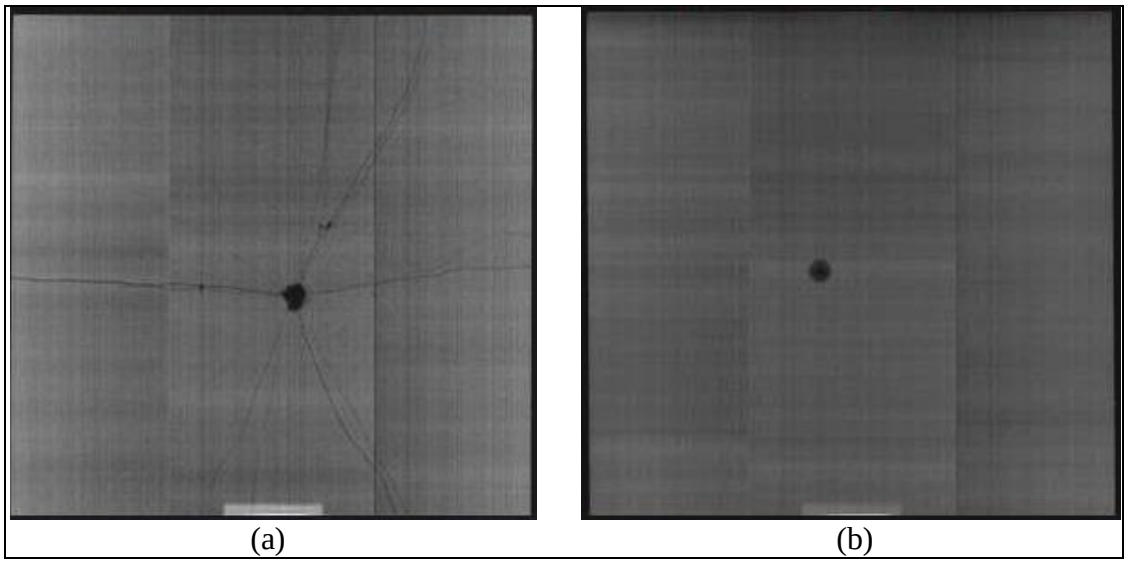

Figure 1. Through-thickness DRs: (a) specimen 740-1 and (b) specimen 741-2.

the DRs. Much of the cracking that was clearly visible by eye in the transparent plates was not visible in the DRs. This is probably due to a combination of very small or no crack width (i.e., "kissing" cracks) and orientation of the cracks relative to the through-thickness direction of the DRs.

3. XCT Scanning Procedures

Each specimen was placed and stabilized on the turntable in a mechanical vice, with its faces in a vertical orientation for computed tomography (CT) scanning. Thus, the specimen faces were perpendicular to the horizontal x-ray (collimated) fan beam, resulting in through-thickness, cross-sectional images. Each specimen was scanned through the approximate center of its impact cavity as well as at vertical locations above and below the centerline of the cavities. Each specimen was scanned using the 420-keV x-ray tube and LDA set up in TR mode. The vertically spaced scans had a slice thickness of 1.000 mm, and each slice was reconstructed to a 1024 × 1024 image matrix. The field of reconstruction diameter was 380.00 mm. The tube energy and current used were 400 keV and 2.0 mA, respectively, and the focal spot was 0.80 mm. The SOD and SID were 649.74 and 948.83 mm, respectively.

4. XCT Evaluation of Specimens

Specimens 740-1 and 741-2 were part of a larger panel set that also included specimens 740-2 and 741-1. Both series of specimens (740 and 741) had one panel struck by a 19.05-mm steel sphere and one panel struck by a 5.56-mm steel sphere. Figure 2 shows the XCT scans through the centerline of the impact cavities of all four specimens. Specimens 740-1 and 741-2 exhibit cone cracks in the middle transparent layer, whereas specimens 740-2 and 741-1 do not. There appears to be multiple cone crack fronts in specimen 741-2. Figure 3 shows an enlarged image of the cone cracks in specimen 740-1 through the centerline as well as images above and below the centerline. Figure 4 shows a series of enlarged images of the cone cracks in specimen 741-2. Figure 4a is through the centerline, and figures 4b–i are 3.6 mm above, 7.2 mm above, 15.0 mm above, 25.6 mm above, 3.6 mm below, 7.2 mm below, 15.0 mm below, and 25.4 mm below the centerline, respectively. The cone crack in specimen 740-1 exhibits a single front, with multiple branches to the left of the impact cavity, which is on the right from the perspective of the incoming threat. The cone cracks in specimen 741-2 exhibit two major fronts, with branching on both sides of the impact cavity. The cracks in both specimens are in their middle plates, with the cracks in 741-2 extending directly from the bottom of the impact cavity in CT scans relatively vertically close to the centerline. The depth of the impact cavity in specimen 741-2 is beyond the relatively thin front ceramic plate.

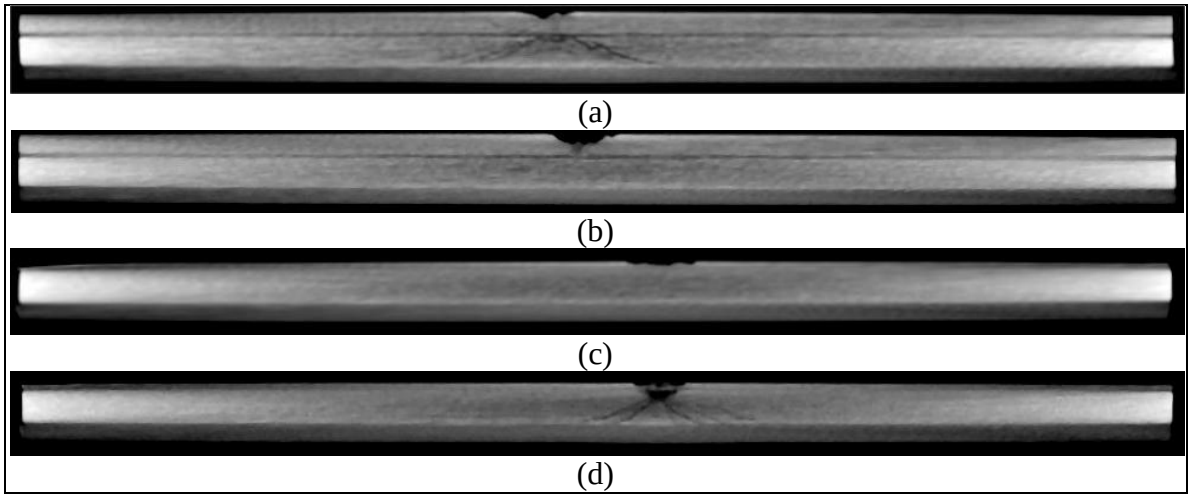

Figure 2. Impact cavity centerline XCT scans (images): (a) specimen 740-1, (b) specimen 740-2, (c) specimen 741-1, and (d) specimen 741-2.

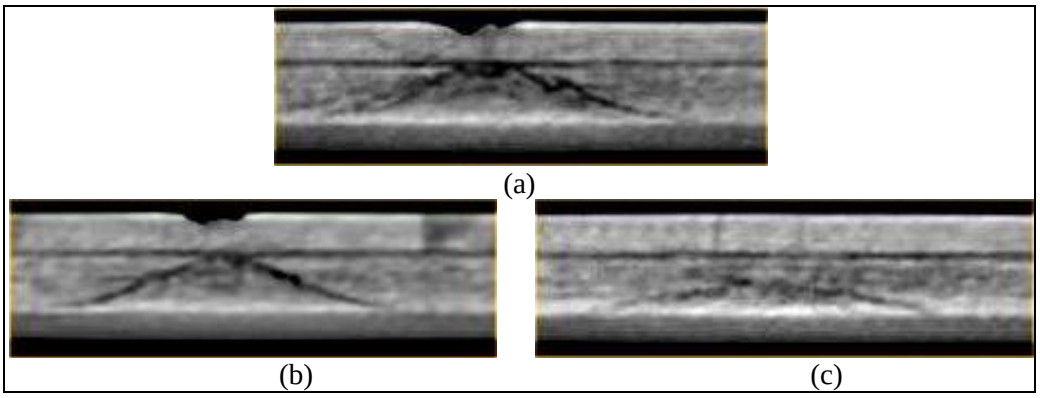

Figure 3. Enlarged XCT scans of specimen 740-1: (a) centerline, (b) 7.7 mm above centerline, and (c) 19.2 mm below centerline.

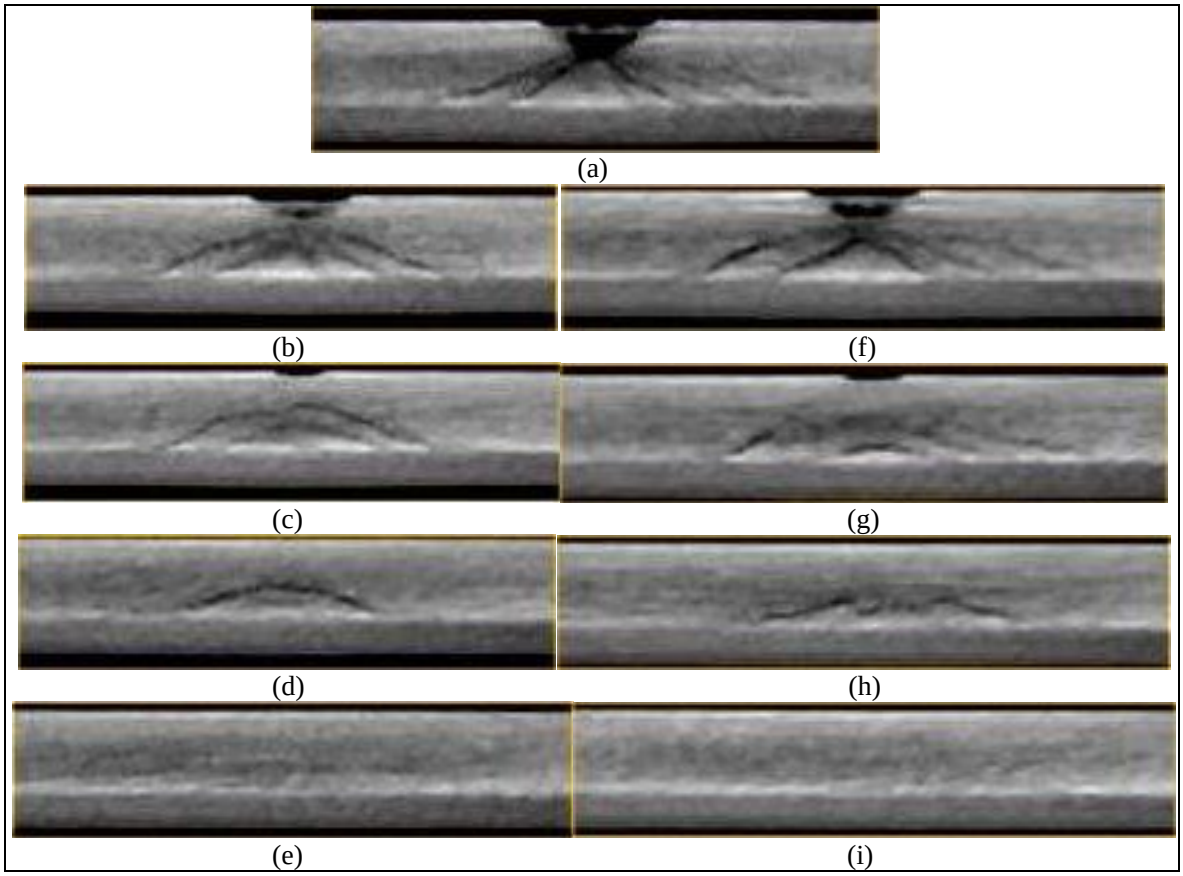

Figure 4. Enlarged XCT scans of specimen 741-2: (a) centerline and (b–i) 3.6 mm above centerline, 7.2 mm above, 15.0 mm above, 25.6 mm above, 3.6 mm below, 7.2 mm below, 15.0 mm below, and 25.4 mm below.

A 3-D point cloud is a set of points in space that define geometrical characteristics (i.e., shape, size, location) of a specimen or scanned volume and features within it. Location of the points is routinely determined by appropriate (image) segmentation of the feature or features of interest. However, if image artifacts are severe enough, they can make it very difficult, if not impossible,

to determine and apply a segmentation approach using only a single (gray) level. Likewise, CT images of specimens with relatively high width-to-thickness ratios (i.e., aspect ratios), which 740-1 and 741-2 have, can be very difficult, if not impossible, to singularly segment or properly spatially separate the gray levels due to nonuniform x-ray beam hardening effects. Figure 5 shows the centerline CT image of specimen 740-1, where critical locations defining beginning, terminating, and intermediate points of the crack and impact cavity are individually marked. Each point is listed below the image in table 1 in (x, y, z) format. Figure 6 shows the centerline CT image of specimen 741-2, where critical locations of the cracks and impact cavity are individually marked. Each point is listed below the image in table 2 in (x, y, z) format. This approach was used because single-level segmentation was not successful with these images, mainly due to the nonuniform beam hardening. Beginning, terminating, and intermediate points of the cracks and impact cavities in each CT image for both specimens were determined. This data set was used to generate curvilinear representations of the cone cracks and their branches and the impact cavities in both specimens (*12*). The points defining the corners of the ceramic plates in both specimens were also determined.

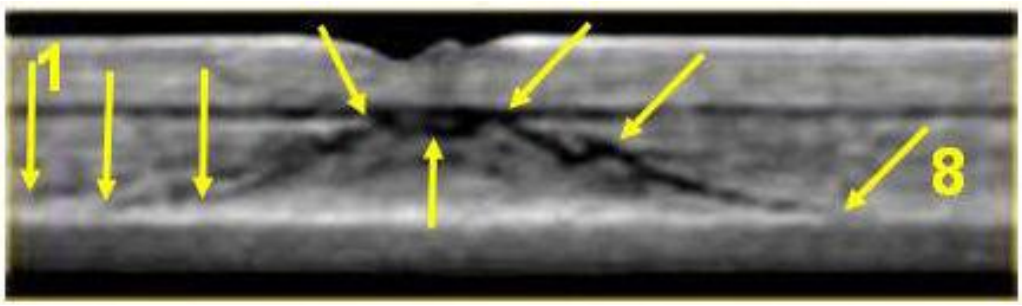

Figure 5. Centerline XCT scan of specimen 740-1, with defining locations of internal crater and cracks marked (arrows).

Table 1. Specific crack and crater locations in specimen 740-1.

Point No.	x Position (mm)	y Position (mm)	z Position (mm)
1	48.80	3.34	210.00
2	42.30	5.57	210.00
3	31.36	3.34	210.00
4	17.44	–4.64	210.00
5	13.73	–2.78	210.00
6	8.54	–4.08	210.00
7	0.74	–0.74	210.00
8	–20.22	5.75	210.00

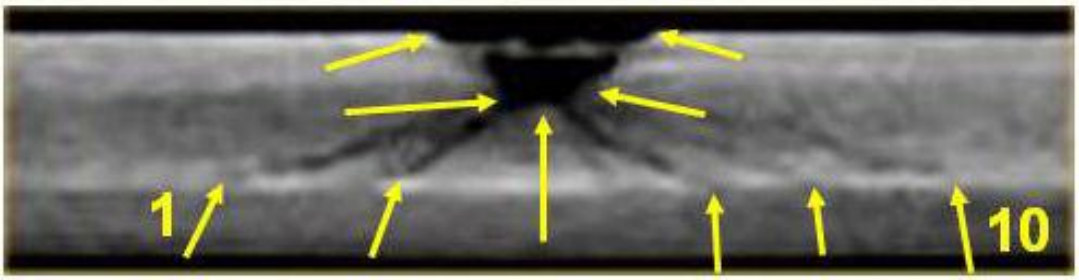

Figure 6. Centerline XCT scan of specimen 741-2, with defining locations of internal crater and cracks marked (arrows).

Table 2. Specific crack and crater locations in specimen 741-2.

Point No.	x Position (mm)	y Position (mm)	z Position (mm)
1	2.01	3.11	227.40
2	–8.97	3.48	227.40
3	–13.55	–8.24	227.40
4	–18.49	–3.48	227.40
5	–20.69	–2.75	227.40
6	–23.44	–3.48	227.40
7	–29.66	–8.42	227.40
8	–34.97	3.48	227.40
9	–41.20	3.30	227.40
10	–52.00	2.75	227.40

Figure 7a is an isometric view of the curvilinear cone cracks in the CT scans of specimen 740-1, where edges of the front and middle ceramic plates are shown in wire frame mode and dashed lines indicate rear or blocked view edges. The backing plate is not shown. Secondly, only a portion of the full vertical height of the specimen is shown, roughly centered on the cracks, in order to show where the cracks are relative to the front and back of the ceramic plates. Together, the cracks roughly define the front or cone shape of the overall 3-D planar crack that goes through the middle ceramic plate. Figure 7b is an isometric view of the cracks in specimen 740-1, showing the location of the front surface of the middle ceramic plate. It is evident that the cracks are mainly in the middle ceramic plate. The curvilinear crack representations were used to generate surfaces over them by a mathematical process called "lofting" (*12*). Figures 8a and b show isometric views of a meshed and solid surface, respectively, giving the overall 3-D geometry of the wide cone-shaped crack in the middle ceramic plate. The slightly recessed region, or "dimple," in the middle of the surfaces is evident in the centerline CT scan of the specimen.

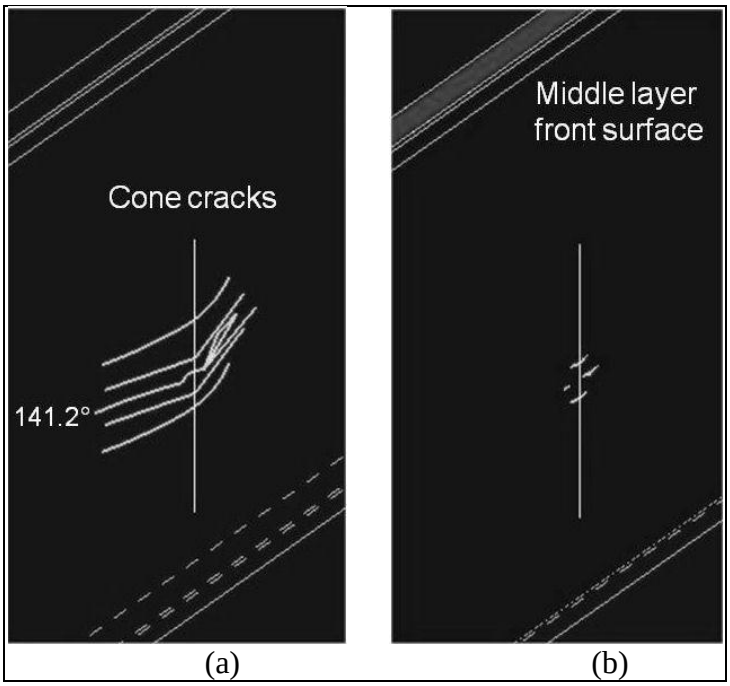

Figure 7. Three-dimensional isometric views of in-plane curvilinear sections of the main cone crack in specimen 740-1: (a) faces of plates displayed as transparent and (b) front surface of middle plate displayed as opaque.

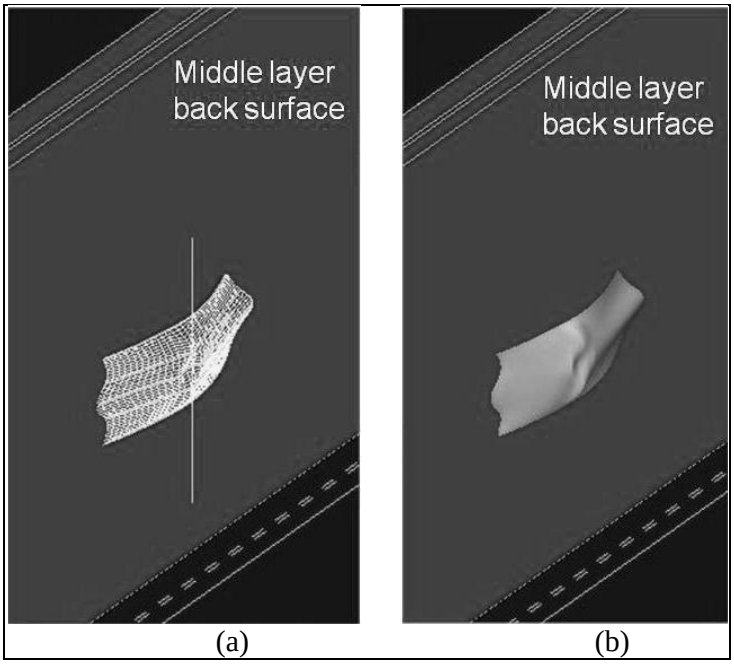

Figure 8. Three-dimensional isometric views of fitted surfaces through the main cone crack in specimen 740-1: (a) meshed surface and (b) solid surface.

Figures 9a–d are a series of isometric views of the curvilinear cracks in the CT scans of specimen 741-2, where edges of the ceramic plates are shown in wire frame mode and dashed lines indicate rear or blocked view edges. Again, only a portion of the full vertical height of the specimen is shown, roughly centered on the cracks, in order to show where the cracks are relative to the ceramic plates. In this case, the front or strike, middle, and backing plates are all shown. Figures 9a, b, and c show all of the mapped crack damage and impact cavity, only the first front of cracks and the impact cavity, and a second front of cracks (behind the first front) and the impact cavity, respectively. In figure 9d, opaque planar surfaces were generated over the front and back face of the middle ceramic plate, along with a planar surface over the back face of the back ceramic plate. This representation clearly shows that the crack damage is in the middle ceramic plate. As was done for specimen 740-1, lofted surfaces were generated from the curvilinear crack representations. Figures 10a and b show isometric views of meshed and opaque versions of the surface through the frontal cracks, respectively. Planar surfaces were generated over the back faces of the middle and back ceramic plates. The shape of the damage cavity produced by the impact is clearly visible in front of the relatively wide cone crack. Figure 10c shows an isometric view of the opaque version of the surface through the second front of cracks. Figure 10d shows an isometric view of the frontal and second surfaces. The frontal surface is meshed, whereas the second surface is opaque, in order to see both. Again, planar surfaces were generated over the back faces of the middle and back ceramic plates. Figure 10e shows an isometric rear view of the frontal and second surfaces, where the second surface is meshed and the frontal surface is opaque. In this case, only the front face of the middle ceramic plate is gridded to emphasize the two major crack surfaces behind it.

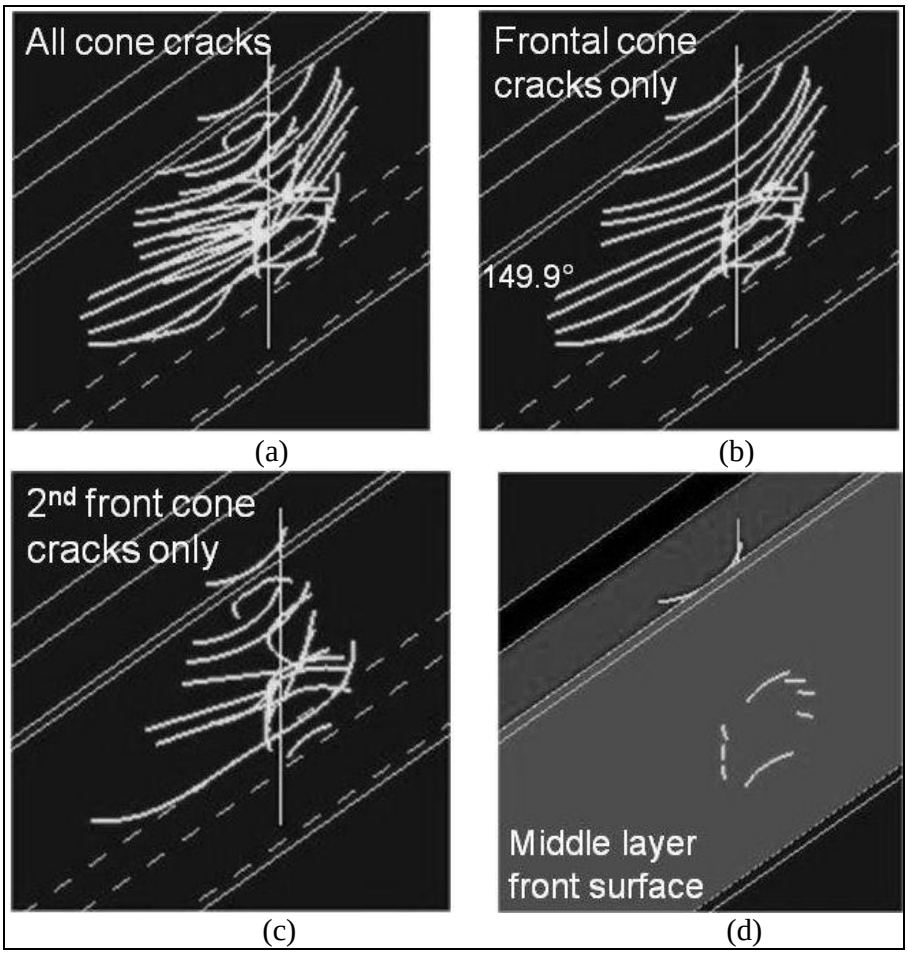

Figure 9. Three-dimensional isometric views of in-plane curvilinear sections of cone cracks in specimen 741-2: (a) all mapped curvilinear sections, (b) only sections of frontal cone crack, (c) only sections of second cone crack, and (d) specific faces of plates are displayed as opaque.

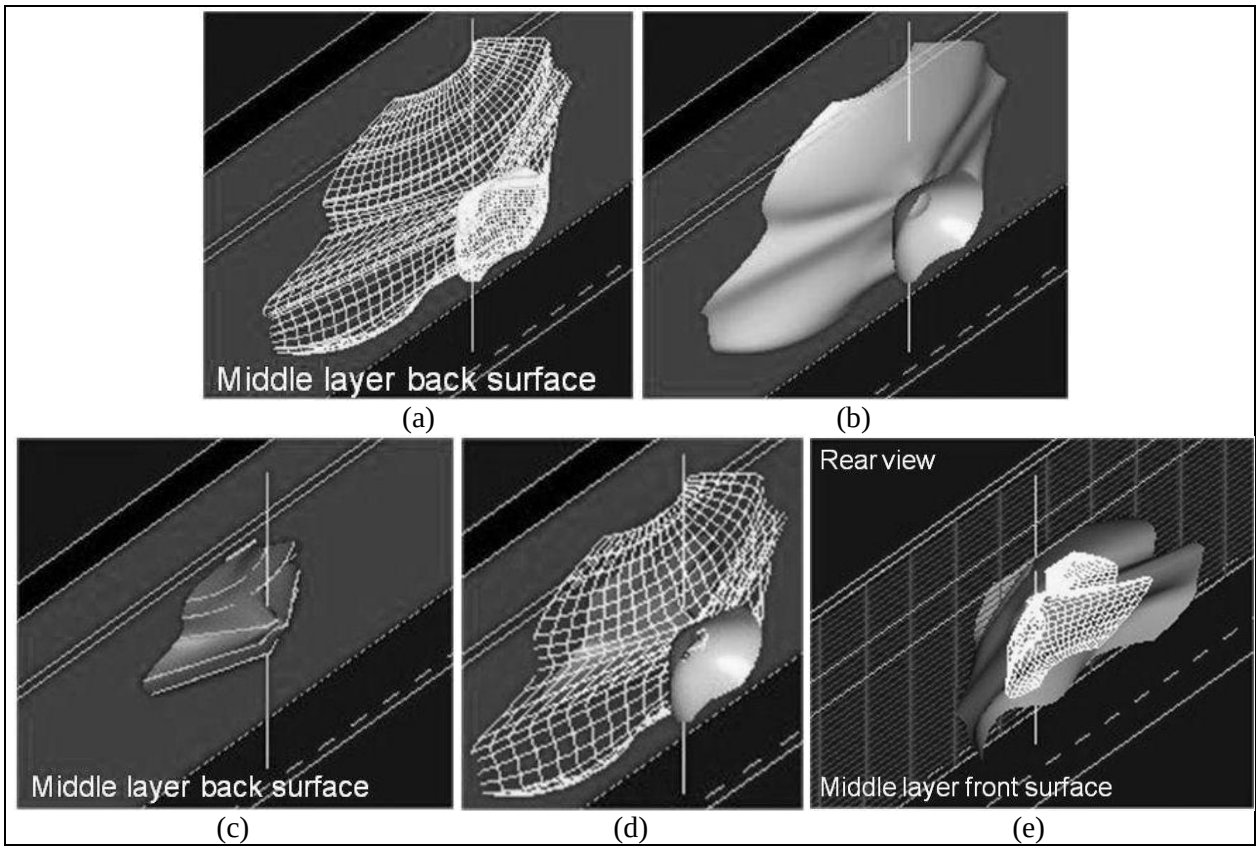

Figure 10. Three-dimensional isometric views of fitted surfaces through cone cracks in specimen 741-2: (a) meshed surface through frontal cone crack, (b) solid surface through frontal cone crack, (c) solid surface through second cone crack, (d) frontal and second cone crack, and (e) rear view of frontal and second crack.

5. Description of Damage Modeling

The ballistic behavior of all targets, which consisted of glass and polycarbonate (PC) backing and were held together by polyurethane and impacted by steel spheres of 19- and 5.56-mm diameter, were simulated using the nonlinear ANSYS/AUTODYN commercial package (*13*). The geometry of the two-dimensional (2-D) and 3-D axisymmetric modeled laminates was identical to the actual geometry of the laminates. Smooth particle hydrodynamics solver was used for the laminate and the impactor. The element size was 0.2 mm for 2-D modeling and 0.5 mm for 3-D modeling. The PC was simply supported at the corners by applying zero velocity along the x-direction as a boundary condition. Results were obtained by simulating a projectile impacting the targets at a constant velocity of 400 and 30 m/s, respectively. The material models used for all materials were obtained from the AUTODYN material library (*13*). The PC was modeled using a shock equation of state (EOS), piecewise Johnson-Cook (JC) strength model, and a plastic strain failure criterion. The projectile steel was modeled using a

shock EOS and a JC strength model. The glass was modeled using a polynomial EOS and Johnson-Holmquist strength and failure models. The polyurethane was modeled using a linear EOS, elastic strength model and principal stress tensile failure.

6. Comparison of Modeling to XCT Scans

Through-thickness, cross-sectional representations of modeled damage at specific distances from the centerline trajectory of the threat were generated from the 3-D modeling data. The damage was modeled over a 50- × 50-mm area. These damage representations were directly compared to cross-sectional XCT scans at the same locations relative to the threat trajectory centerline. Figure 11 shows a series of modeled damage "slices" and some XCT scans of specimen 740-1 side by side. XCT scans were not done at all of the vertical locations shown by the modeled slices. The modeled slices on the left, which are symmetric above (+) and below (-) the centerline trajectory, are at the centerline position (top picture), followed by ±3.6, ±7.7, ±15.0, ±20.0, and ±25.0 mm. Similarly, the first XCT scan on the right (top picture) is at the centerline position. The other two XCT scans on the right are 7.7 mm above and 19.2 mm below the centerline trajectory. The modeled damage centerline slice shows a small amount of ejecta at the top of the specimen, whereas the XCT scans do not, since it was not present at the time of scanning. The width of the impact cavity or crater in the centerline images is comparable with a width of about 10 mm at the surface in the XCT scan. However, the maximum span of the cone crack at the rear of the middle layer of the specimen is significantly different in the two sets of images.

Table 1 shows that the maximum span of the cone crack is about 70 mm in the XCT scan, whereas it is significantly less in the modeled slice given the 50- × 50-mm area modeled. Both the XCT scans and modeled slices show that the maximum span of the cone crack remains approximately the same, with increased distance from the centerline trajectory. The XCT scans show that the cone crack flattens out relatively gradually and smoothly, with increased distance from the centerline trajectory, whereas the modeled slices predicted more staggered type damage with sharp corners. The modeled slices predicted that horizontal damage in the form of the flattened cone crack would be present about 25 mm above and below the centerline trajectory. The cone crack in the XCT scan at about 19 mm below the centerline trajectory has started to flatten out.

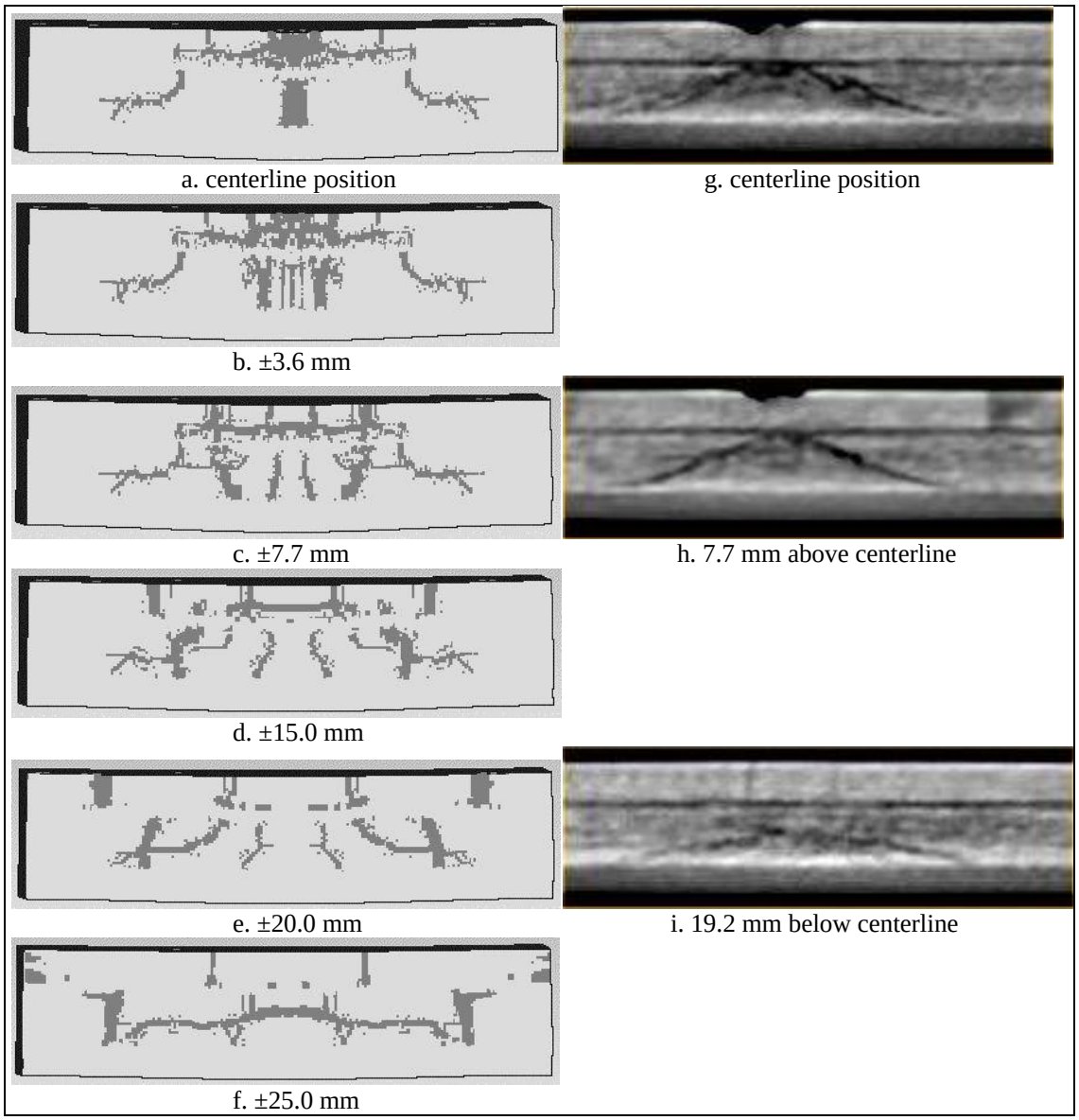

Figure 11. Side-by-side comparison of modeled damage "slices" and XCT scans of specimen 740-1: (a–f) modeled damage and (g–i) XCT scans.

Figure 12 shows a series of modeled damage "slices" and XCT scans of specimen 741-2 side by side. The modeled slices on the left, which are symmetric above (+) and below (–) the centerline trajectory, are at the centerline position (top picture), followed by ±3.6, ±7.2, ±10.0, ±15.0, ±20.0, and ±25.0 mm. Similarly, the first XCT scan on the right (top picture) is at the centerline position. However, the actual damage is not exactly symmetric about the centerline trajectory, as might be expected. The following XCT scans on the right are 3.6 mm above, 7.2 mm above, 15.0 mm above, 15.0 mm below, 25.0 mm above, and 25.0 mm below the centerline trajectory. The modeled damage slices show the ejecta, whereas the XCT scans do not, since it was not present at the time of scanning. The width of the impact cavity or crater in the centerline images is similar, with a width of about 16 mm at the surface in the XCT scan. Secondly, the changes in

the width and depth of the impact cavity in the XCT scans from the centerline position to 7.2 mm above the centerline are reflected in the modeled slices. The XCT scans also show a distinct two-front, cone-cracking type of damage (+3.6, +7.2, + 15.0 mm), which is also clearly reflected in the modeled slices (±3.6, ±7.2, ±10.0 mm).

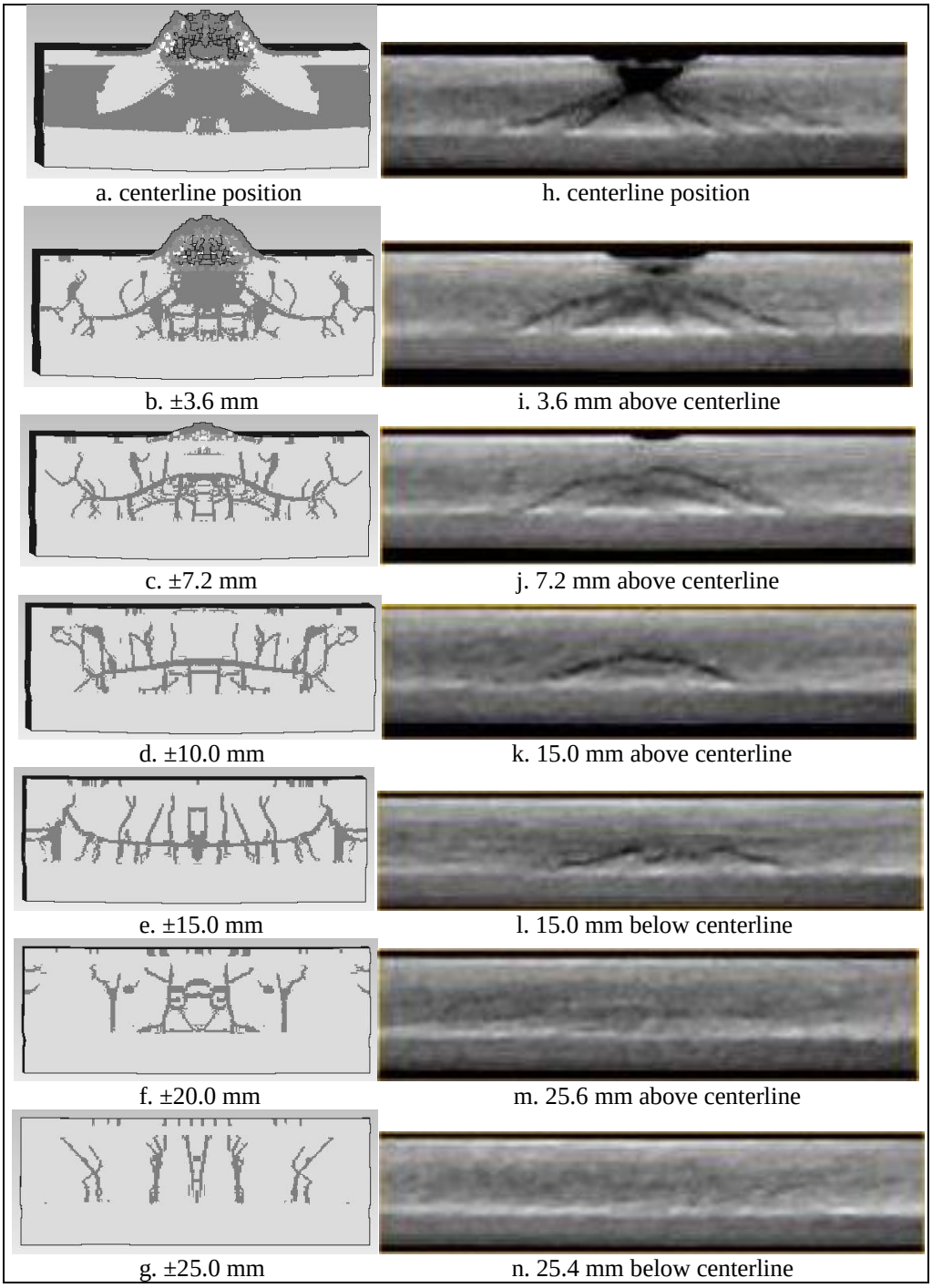

Figure 12. Side-by-side comparison of modeled damage slices and XCT scans of specimen 741-2: (a–g) modeled damage and (h–n) are XCT scans.

Both the XCT scans and modeled slices show the gradual flattening out of the cone crack fronts towards the rear of the specimen away from the centerline trajectory. At ±15.0 mm in the modeled slices, the main horizontal crack is inverted, which has occurred, to some extent, to the cone crack front in the XCT scan at –15.0 mm. Lastly, the XCT scans show that there is very little or no cone-crack type damage at about 25 mm above and below the centerline trajectory, which is reflected in the modeled slices at ±25.0 mm. However, the XCT scans do not show the same level of through-thickness type cracking that is apparent in the modeled slices. The through-thickness cracks have approximately the same width as the cone cracks in the modeled slices, so it is possible that the through-thickness type cracking in the specimen is not as severe as the modeled slices suggest it would be.

7. Conclusions

Cone cracks in multilayered transparent panel structures were characterized and analyzed using x-ray computed tomography and 3-D visualization tools. Cone cracks in specimens 740-1 and 741-2, which were struck by a 19.05-mm-diameter steel sphere with an impact velocity of 32.4 m/s and a 5.56-mm-diameter steel sphere with an impact velocity of 405 m/s, respectively, were evaluated. Cone crack location data in individual XCT scans was used to generate curvilinear representations of the cracks, which were presented in 3-D isometric, wireframe-type views, with the edges of the individual ceramic plates for spatial reference. Three-dimensional cone crack surfaces, or fronts, were generated from the (in-plane) curvilinear representations by a process called lofting. The 3-D visualizations of the cone crack fronts clearly showed their locations, sizes, and angles, or trajectories, within the multilayered structure of the panels. Individual cross-sectional XCT scans were directly compared to through-thickness cross-sectional representations of modeled damage at corresponding locations. Overall, agreement between the XCT scans and the modeled damage was fair in specimen 740-1, with the XCT scans showing a significantly wider maximum cone crack span at the rear of the middle layer of the specimen. Agreement between the XCT scans and the modeled damage was good in specimen 741-2, with the modeled damage predicting more extensive, short, through-thickness cracking than was evident in the XCT scans.

8. References

1. Green, W.; Miller, H.; LaSalvia, J.; Dandekar, D.; Casem, D. Evaluation of Ballistically-Induced Damage in Ceramic Targets by X-ray Computed Tomography. *Proceedings of 32nd International Conference on Advanced Ceramics and Composites - Topics in Ceramic Armor, Advances in Ceramic Armor IV,* 2008; Vol. 29, pp 195–206.

2. Miller, H. T.; Green, W. H.; LaSalvia, J. C. Ballistically-Induced Damage in Ceramic Targets as Revealed by X-ray Computed Tomography. *Proceedings of 31st International Conference on Advanced Ceramics and Composites - Topics in Ceramic Armor, Advances in Ceramic Armor III,* 2007; Vol. 28, pp 193–202.

3. Bourne, N.; Green, W.; Dandekar, D. On the One-Dimensional Recovery and Microstructural Evaluation of Shocked Alumina. *Proceedings of the Royal Society A: Mathematical, Physical, and Engineering Sciences*, 2006.

4. Wells, J.; Brannon, R. Advances in X-Ray Computed Tomography Diagnostics of Ballistic Impact Damage. *Metallurgical and Materials Transactions A* **2007**, *38A*, 2944–2949.

5. Wells, J. Progress in the Nondestructive Analysis of Impact Damage in TiB_2 Armor Ceramics. *Proceedings of 30th International Conference on Advanced Ceramics and Composites - Topics in Ceramic Armor, Advances in Ceramic Armor II*, 2006; Vol. 27, pp 198–209.

6. Wells, J.; Rupert, N.; Neal, M. Impact Damage Analysis in a Level III Flexible Body Armor Vest Using XCT Diagnostics. *Proceedings of 33rd International Conference on Advanced Ceramics and Composites - Topics in Ceramic Armor, Advances in Ceramic Armor V*, 2009; pp. 171–182.

7. Green, W.; Carter, R. Evaluation of Ballistic Damage in an Encapsulated Ceramic Panel via X-ray Computed Tomography. *Proceedings of Review of Progress in Quantitative NDE, AIP Conference Proceedings*, 2009; Vol. 1096, pp 1099–1106.

8. Green, W.; Brennan, R.; Carter, R. Nondestructive Evaluation of as Fabricated and Damaged Encapsulated Ceramics. *Proceedings of 33rd International Conference on Advanced Ceramics and Composites - Topics in Ceramic Armor, Advances in Ceramic Armor V,* 2009; Vol. 30, pp 147–158.

9. Brennan, R.; Green, W. Low Velocity Impact Testing and Nondestructive Evaluation of Transparent Materials. *Proceedings of Review of Progress in Quantitative NDE, AIP Conference Proceedings*, 2011; Vol. 1335, pp 965–972.

10. Green, W.; Brennan, R.; Fountzoulas, C. Current NDE Studies of Impact Damage in Multi-Layered Transparent Panel Structures. Presented at *Materials Science & Technology 2011 Conference and Exhibition*, Columbus, OH, October 2011.

11. Wells, J. XCT Diagnostics of Ballistic Impact Damage in Transparent Armor Targets. Presented at the *36th International Conference on Advanced Ceramics and Composites - Topics in Ceramic Armor, Advances in Ceramic Armor VIII*, Daytona Beach, FL, 2012.

12. SDRC/Imageware. Basic Reverse Engineering with Surfacer: Training Guide; pp 326–327 and 336–337, March 1999.

13. Century Dynamics Inc. ANSYS/AUTODYN manual; Vol. 12.0, Concord, CA, 2009.

NO. OF COPIES	ORGANIZATION
1 (PDF only)	DEFENSE TECHNICAL INFORMATION CTR DTIC OCA 8725 JOHN J KINGMAN RD STE 0944 FORT BELVOIR VA 22060-6218
1	DIRECTOR US ARMY RESEARCH LAB IMAL HRA 2800 POWDER MILL RD ADELPHI MD 20783-1197
1	DIRECTOR US ARMY RESEARCH LAB RDRL CIO LL 2800 POWDER MILL RD ADELPHI MD 20783-1197

NO. OF
COPIES ORGANIZATION

ABERDEEN PROVING GROUND

8 DIR USARL
RDRL WMM B
C FOUNTZOULAS
RDRL WMM D
R BRENNAN
R CARTER
E CHIN
W GREEN (3 CPS)
M PEPI